Title	INTRINSIC SHAPE OF STAR-FORMING BzK GALAXIES AT z ~ 2 IN GOODS-N
Author(s)	Yuma, Suraphong; Ohta, Kouji; Yabe, Kiyoto; Kajisawa, Masaru; Ichikawa, Takashi
Citation	The Astrophysical Journal (2011), 736(2): 92
Issue Date	2011-07
URL	http://hdl.handle.net/2433/147140
Right	© 2011. The American Astronomical Society.
Type	Journal Article
Textversion	author

INTRINSIC SHAPE OF STAR-FORMING BZK GALAXIES AT $Z \sim 2$ IN GOODS-N

Suraphong Yuma [1], Kouji Ohta [1], Kiyoto Yabe [1], Masaru Kajisawa [2], Takashi Ichikawa [3]

Draft version September 22, 2011

ABSTRACT

We study structure of star-forming galaxies at $z \sim 2$ in GOODS-N field selected as sBzK galaxies down to $K_{AB} < 24.0$ mag. Among 1029 sBzK galaxies, 551 galaxies (54%) show a single component in ACS/F850LP image obtained with the Hubble Space Telescope; the rest show multiple components. We fit the single-component sBzK galaxies with the single Sérsic profile using the ACS/F850LP image and find that a majority of them (64%) show Sérsic index of $n = 0.5 - 2.5$, indicating that they have a disk-like structure. The resulting effective radii typically range from 1.0 to 3.0 kpc in the rest-frame UV wavelength. After correcting the effective radii to those in the rest-frame optical wavelength, we find that the single-component sBzK galaxies locate in the region where the local and $z \sim 1$ disk galaxies distribute in the stellar mass-size diagram, suggesting comparable surface stellar mass density between the sBzK and $z \sim 0 - 1$ disk galaxies. All these properties suggest that the single-component sBzK galaxies are progenitors of the present-day disk galaxies. However, by studying their intrinsic shape through comparison between the observed distribution of apparent axial ratios and the distribution for triaxial models with axes ($A > B > C$), we find that the mean B/A ratio is $0.61^{+0.05}_{-0.08}$ and disk thickness C/A is $0.28^{+0.03}_{-0.04}$. This indicates that the single-component sBzK galaxies at $z \sim 2$ have a bar-like or oval shape rather than a round disk shape. The shape seems to resemble to a bar/oval structure that form through bar instability; if it is the case, the intrinsic shape may give us a clue to understand dynamical evolution of baryonic matter in a dark matter halo.

Subject headings: galaxies: evolution — galaxies: formation — galaxies: high-redshift — galaxies: structure

1. INTRODUCTION

Formation of disk galaxies is one of the important problems in astronomy. Many theoretical studies proposed scenarios of the disk formation through analytical approaches (e.g., White & Rees 1978; Fall & Efstathiou 1980) or simulations (e.g., Navarro & Benz 1991; Navarro & White 1994; Navarro & Steinmetz 1997; Barnes 2002; Springel & Hernquist 2005; Robertson et al. 2006; Sales et al. 2010; Dutton et al. 2011). However, formation epoch of disks and high-redshift counterparts of the present-day disk galaxies are still not clear. Observational studies have been revealing that disk galaxies are already in place at $z \sim 1$. Although a mild luminosity evolution (~ 1 mag) can be seen up to $z \sim 1$ (e.g., Brinchmann et al. 1998; Scarlata et al. 2007), stellar mass-size relation does not change significantly (Barden et al. 2005). Stellar-mass function of disk galaxies also does not evolve so much up to $z \sim 1$ in the massive part (e.g., Bundy et al. 2005; Pannella, et al. 2006). Furthermore, disk-size (scale length for the exponential law) function does not show significant evolution for the larger disks (Lilly et al. 1998; Sargent et al. 2007). These suggest that the formation of disk galaxies is beyond $z \sim 1$. Meanwhile, no clear counterparts of disk galaxies are known at $z > 3$. Some of Lyman break galaxies (LBGs) at $z \sim 3$ show the surface brightness distribution with Sérsic index of $n \sim 1$ (e.g., Steidel et al. 1996). Akiyama et al. (2008) found that most of their LBG sample at $z \sim 3$ show Sérsic profiles with $1 < n < 2$ in the rest-frame optical wavelength by AO-assisted $K-$band imaging obser-

vations. They showed, however, that the stellar-mass density is too high to evolve into the present-day disk galaxies, suggesting that the LBGs are progenitors of elliptical galaxies. Furthermore, clustering amplitude of LBGs is very large indicating that they reside in massive dark halos and their destination would be giant elliptical galaxies in rich clusters (e.g., Ouchi et al. 2001; Giavalisco & Dickinson 2001). Thus LBGs (at least bright/massive LBGs) are presumably not a direct progenitor of present-day disk galaxies. In other words, no obvious disk galaxy existed at $z > 3$. In fact, Kajisawa & Yamada (2001) studied a nearly complete sample of galaxies to $z = 2$ and found that the Hubble sequence was established during $z \sim 1 - 2$ epoch, though the sample size is not large.

Therefore, the epoch of $z \sim 2$ is important for the understanding of disk formation. The redshift range is, however, so-called redshift desert, and isolating galaxies at the epoch is not easy. Daddi et al. (2004) proposed a two-color selection method to isolate galaxies at $1.4 \lesssim z \lesssim 2.5$ by using $B - z'$ and $z' - K$ colors. Galaxies selected by this method are called BzK galaxies. Star-forming BzK (sBzK) and passive BzK (pBzK) are defined according to the location of a galaxy in the $B - z'$ and $z' - K$ diagram (Daddi et al. 2004). Properties of BzK galaxies have been studies (e.g., Daddi et al. 2004, 2005; Kong et al. 2006; Hayashi et al. 2007; Hartley et al. 2008; Yoshikawa et al. 2010). Among them, Hayashi et al. (2007) studied the clustering properties of faint sBzK galaxies ($K_{AB} < 23.2$ mag) and found that they reside in halos with a typical mass of $\sim 3 \times 10^{11} M_\odot$, which is comparable to the halo mass of the local disk galaxies (see also Ichikawa et al. 2007). This suggests that they are likely to be progenitors of the present-day disk galaxies if no major merge occurs at later time. With the SINS survey (Förster Schreiber et al. 2006), Förster Schreiber et al. (2009) studied the kinematical properties of 80 galaxies at $1.3 < z < 2.6$ including BM/BX and sBzK galaxies. They derived velocity structure

Electronic address: yuma@kusastro.kyoto-u.ac.jp

[1] Department of Astronomy, Kyoto University, Sakyo-ku, Kyoto 606-8502, Japan

[2] Research Center for Space and Cosmic Evolution, Ehime University, Bunkyo-cho, Matsuyama, 790-8577, Japan

[3] Astronomical Institute, Tohoku University, Aoba, Sendai 980-8578, Japan

using Hα emission line and found that about one-third of their sample galaxies are rotation-dominated disks which follow a velocity-size relation similar to local disk galaxies. However, these galaxies show larger velocity dispersion than local disks, maybe suggesting the thicker disk. These observational results seem to suggest that star-forming galaxies at $z \sim 2$ are disk galaxies with a thicker disk. However, no study of the intrinsic shape of these galaxies has been established yet.

The intrinsic structure of galaxies is related to the apparent axial ratio (b/a) or ellipticity ($1 - b/a$) of galaxies. In the local universe, it is found that elliptical and disk galaxies have different observed axial ratio distributions. The distribution for local elliptical galaxies peaks at $b/a \sim 0.8$ and decreases to zero at $b/a = 0.2$, whereas disk galaxies show a rather flat distribution in the range of $b/a = 0.2-0.8$ (e.g., Lambas et al. 1992; Padilla & Strauss 2008; Unterborn & Ryden 2008). In this paper, we constrain the intrinsic three-dimensional structure of star-forming BzK galaxies at $z \sim 2$ from their observed axial ratios in order to investigate whether they indeed have a disk structure or not.

This paper is organized as follows. Section 2 describes the optical-to-mid-infrared data sources used in this study. In Section 3, we construct a sample of sBzK galaxies and derive their photometric redshifts and stellar masses. The morphological analysis is described in section 4. Then we examine the intrinsic shape of the sBzK galaxies from their distributions of apparent axial ratios in section 5. The possible origin and evolution of the intrinsic structure are discussed in section 6. Conclusion is presented in section 7. Throughout this paper, we use the AB magnitude system (Oke et al. 1983) and assume a standard ΛCDM cosmology with parameters of $\Omega_m = 0.3$, $\Omega_\Lambda = 0.7$, and $H_0 = 70$ km s^{-1} Mpc^{-1}.

2. DATA SOURCES

We used the publicly available images in U, B, V, R, I_c, and z' bands in the Great Observatories Origins Deep Survey North (GOODS-N) field (Capak et al. 2004)[4]. The U-band image was obtained with the MOSAIC prime focus camera on the Kitt Peak National Observatory (KPNO) 4m telescope. The B-, V-, R-, I_c-, and z'-band images were obtained with Suprime-Cam attached to the Subaru telescope. Details of the data reduction can be found in Capak et al. (2004). The seeing sizes of U-, B-, V-, R-, I_c-, and z'-band images are 1.″3, 1.″1, 1.″1, 1.″2, 1.″1, and 1.″1, respectively and the 5σ limiting magnitudes at 3″ diameter aperture are 26.5, 26.0, 25.7, 25.8, 25.1, and 24.8 mag, respectively.

In order to study the morphology of sBzK galaxies, we used the high resolution image observed with Advanced Camera for Surveys (ACS) on the Hubble Space Telescope (HST). The F850LP image (hereafter referred as z_{850} image) was obtained from the HST/ACS v2.0 data products of the GOODS HST/ACS treasury program (Giavalisco et al. 2004)[5] and covered an area of ~ 160 arcmin^2. The pixel scale of the image is 0.″03 pixel^{-1}. The full width at half maximum (FWHM) of the point-spread function (PSF) is $\sim 0.″11$. The 5σ limiting magnitude of the z_{850} image is 26.5 mag at 1.″0 diameter aperture.

For the near-infrared (NIR) data, we used very deep and wide J-, H-, and K-band data obtained with Multi-Object InfraRed Camera and Spectrograph (MOIRCS; Suzuki et al. 2008) on the Subaru telescope, i.e., MOIRCS Deep Survey

(MODS; Kajisawa et al. 2006; Ichikawa et al. 2007). Four MOIRCS pointings cover $\sim 70\%$ of the GOODS-N region (103.3 arcmin^2, hereafter "wide field"; Kajisawa et al. 2009). One of the four pointings includes the Hubble Deep Field North (HDF-N; Williams et al. 1996) and is the deepest field of the MODS (hereafter deep field). The FWHM of the PSF is 0.″50 for the deep field and 0.″61 for the wide field. The images reach $J = 25.3$, $H = 24.6$, and $K = 25.1$ mag (5σ at 1.″2 diameter aperture) for the wide field and $J = 26.0$, $H = 24.9$, and $K = 25.7$ mag for the deep field.

Mid-infrared images were obtained from deep observations with the Infrared Array Camera (IRAC) on the Spitzer Space Telescope (SST). We used 3.6 and 4.5μm band images from the First (DR1) and Second Data Release (DR2) of the publicly available data provided by the SST Legacy Science program[6]. The pixel scale of all images after being drizzled is 0.″60 pixel^{-1}. The 5σ limiting magnitudes of the IRAC 3.6 and 4.5μm images at 2.″4 diameter aperture are 25.4 and 25.3 mag, respectively.

3. SAMPLE SELECTION AND SED FITTING

In order to select star-forming galaxies at $z \sim 2$ with BzK method, we first made position registrations of B- and z'-band images by using the K-band image as a reference. All images were homogenized to have seeing sizes of 1.″1. Object detection was made in the K-band image with criteria of 5 connections above a 1.5σ minimum threshold by SExtractor version 2.5.0 (Bertin & Arnouts 1996). For each object with MAG_AUTO< 24.0 in K band, the aperture photometry was made for B and z' bands at 1.″6 diameter aperture by using dual-image mode of SExtractor, where the aperture size was found to provide the best signal-to-noise (S/N) ratio for the homogenized images.

Star-forming galaxies at $z \sim 2$ were selected by applying the BzK color criterion for star-forming galaxies (sBzK; Daddi et al. 2004) to the K-selected galaxies down to $K < 24.0$ mag. Since the response functions in our system are not identical to those used by Daddi et al. (2004), we derived the color correction by convolving the empirical stellar spectra from Pickles (1998) with the response functions including the detector's QE and atmospheric transmission. We found that $B - z'$ colors of stars in our system are bluer than those in Daddi et al. (2004) about $0.05 - 0.4$ mag depending on the spectral type, whereas our $z' - K$ colors are 0.02 mag redder on average. In order to apply the BzK criterion consistent with Daddi et al. (2004), we applied the $B - z'$ color correction to all objects by using the following equation;

$$(B - z)_{\mathrm{Daddi}} = (B - z') + 0.4. \qquad (1)$$

Although the offset of 0.4 mag is not valid for all colors of $B - z$, it makes the selection criterion more secure as it is the upper limit offset. We did not correct for the $z' - K$ colors. The original sBzK criterion, $BzK \equiv (z - K) - (B - z) \geq -0.2$, was then applied to construct the sBzK sample. Objects with $z_{spec} < 1.4$ or $z_{spec} > 2.5$ are excluded from the sample based on spectroscopic identifications by Wirth et al. (2004) and Barger et al. (2008). Resulting sample consists of 1029 sBzK galaxies.

In order to study the morphological properties, we cross-matched the sBzK galaxies with the high-resolution z_{850} image, for which the central wavelength corresponds to the rest-
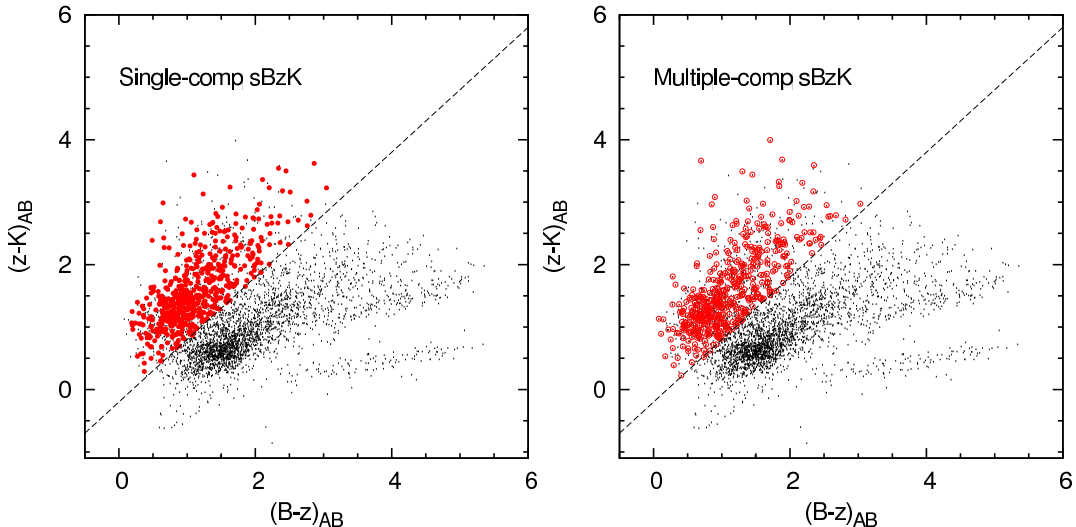
Figure 1. Two-color $(B - z')$ vs. $(z' - K)$ diagram for sBzK galaxies in GOODS-N field. The $B - z'$ color shown here was corrected to match the filter system used by Daddi et al. (2004) (see text for more details). Red solid circles in the left panel represent 551 single-component sBzK galaxies, while red open circles in the right panel show 478 multiple-component objects (section 3). All objects with $K < 24.0$ mag are also shown with dots.

frame UV wavelength of ~ 3000Å at $z \sim 2$. Counterparts of the sBzK galaxies in the z_{850} images are identified if they are detected above 3σ limiting magnitude (27 mag) within $0.''72$ radius centering at the positions of sBzK galaxies in the K-band image. This radius is twice as large as the median $1/2$FHWM of the sample. The sBzK galaxies are divided into 2 groups: sBzK galaxies matched with only one object in the z_{850} image (hereafter single-component objects) and sBzK galaxies matched with more than one object (hereafter multiple-component objects). 551 galaxies are classified as single-component objects and 478 galaxies are multiple-component objects; 54% of the sBzK galaxies show a single structure in the z_{850} image. Figure 1 indicates that the single-component and the multiple-component sBzK galaxies show very similar distributions in the BzK diagram (left and right panel, respectively). In this paper, we concentrate our analysis on single-component objects (red circles in the left panel of Figure 1). K magnitudes and z' magnitudes of the single-component galaxies, which are shown in Figure 2, distribute in the range of $20.0 - 24.0$ mag and $21.0 - 26.0$ mag, respectively. The distributions of all sBzK galaxies are also shown in both panels with open histograms. It is worth noting that as star-forming regions in a face-on galaxy could be seen separately in the rest-frame UV wavelength, it is possible that they are selected as a multiple-component object in this analysis. Study of structure at the rest-frame optical wavelength in the future is helpful to see if they really have multiple components or just star-forming regions in a face-on galaxy.

The photometric redshifts and stellar masses of the single-component sBzK galaxies were obtained by spectral energy distribution (SED) fitting. SEDs of the single-component sBzK galaxies were constructed by the photometry in U, B, V, R, I_c, z', J, H, K, IRAC 3.6μm, and 4.5μm bands. For all but IRAC images, we smoothed the images to match the seeing size of U-band images ($1.''3$) as it has the worst seeing size. Then the aperture photometry was made at $1.''6$ diameter aperture by using dual-image mode. The total magnitudes were obtained by using the correction factor that was determined by scaling the aperture magnitude of each object to the MAG_AUTO in the K-band image. For the IRAC images, we made the aperture photometry without homogeniz-

ing the images at $2.''4$ diameter aperture, which maximizes the S/N. The total magnitudes were obtained by using the aperture correction factor determined for each band. The process of determining the aperture correction factor is identical to that used by Yuma et al. (2010). The aperture photometry at the same aperture size as done for our targets was made for artificial objects with known total magnitudes put into the IRAC images. The correction factors are -0.62 mag and -0.72 mag for 3.6μm and 4.5μm bands, respectively. The photometric redshifts of the single-component sBzK galaxies were obtained with $Hyperz$ (Bolzonella et al. 2000). We checked the accuracy of our photometric redshift estimation using objects with available spectroscopic redshifts (Barger et al. 2008). The comparison between the photometric and the spectroscopic redshifts shows median and standard deviation of $\delta_z \equiv (z_{phot} - z_{spec})/(1 + z_{spec})$ of -0.03 and 0.07, respectively. The histogram of the resulting photometric redshifts is shown in the left panel of Figure 3. Most of the samples have the photometric redshifts between 1.3 and 2.5. Note that although we did not exclude sBzK galaxies with $z_{phot} < 1.3$ or $z_{phot} > 2.5$ from our sample, it does not affect the results. The stellar mass was obtained from SED fitting with z_{phot}. We constructed model SEDs of various star-formation histories (i.e., instantaneous burst, constant star formation, or exponentially declining models) by using the Bruzual & Charlot (2003) synthesis code. Salpeter (1955) initial mass function (IMF) with a mass range of $0.1 - 100$ $M_\odot$ was assumed. The metallicity was fixed at solar abundance. The dust attenuation law of Calzetti et al. (2000) was adopted and $E(B-V)$ range was taken from 0.0 to 1.0 mag with a step of 0.01 mag. The SED fitting process was the same as that used by Yuma et al. (2010). The histogram of stellar masses is shown in the right panel of Figure 3. It is seen that most of the single-component sBzK galaxies have the stellar masses of $10^9 - 10^{11}$ $M_\odot$.

4. MORPHOLOGICAL ANALYSIS

4.1. *Estimation and Accuracy of Sérsic parameters*

We determined the structural parameters of the single-component sBzK galaxies by fitting the two-dimensional light distributions in the z_{850} image with a single Sérsic profile (Sérsic 1963, 1968). The Sérsic profile is expressed by
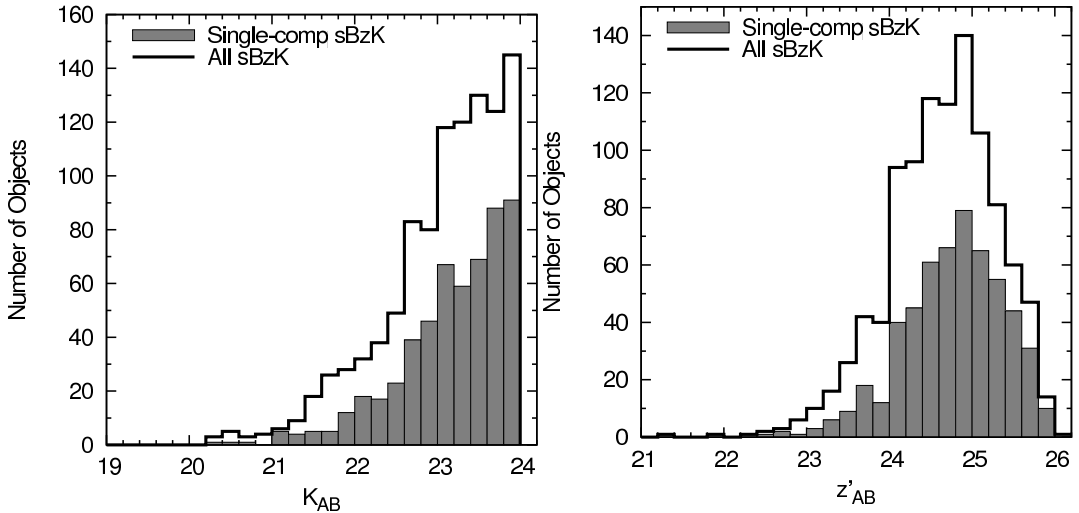
Figure 2. Magnitude histograms of all and single-component sBzK galaxies in K band (left panel) and z' band (right panel). Open histograms are for all sBzK galaxies after removing objects with $z_{spec} < 1.4$ or $z_{spec} > 2.5$, while black shaded histograms represent the single-component sBzK galaxies.
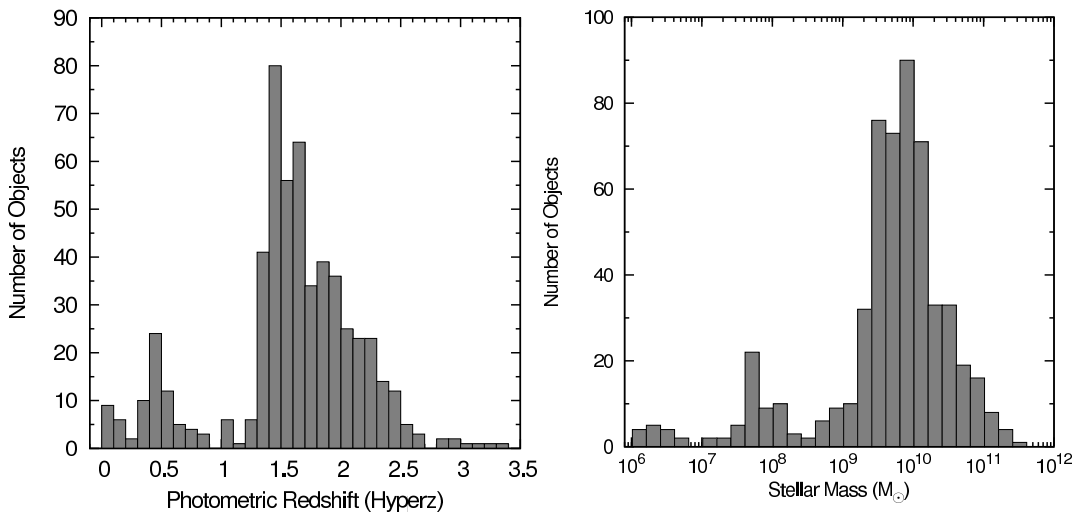

Figure 3. Histograms of photometric redshifts (left panel) and stellar masses (right panel) of the single-component sBzK galaxies.

$I(r) = I_e \exp \left\{ -\kappa_n \left[\left(\frac{r}{r_e} \right)^{1/n} - 1 \right] \right\}$, where I_e is the surface brightness at the effective radius r_e and κ_n is a parameter related to the Sérsic index n. The index n determines the shape of the profile. In the local universe, an exponential profile ($n = 1$) is seen for a disk component, whereas $n \sim 4$ is representative of a spheroid component. The two-dimensional profile fitting was done by using the GALFIT version 2 (Peng et al. 2002). There are seven free parameters which are determined by χ^2 minimization: central position, total magnitude, n, r_e, apparent axial ratio (b/a), and position angle. The Sérsic index n was initially set to be $n = 1.5$. We tested the dependence of final GALFIT results on the initial Sérsic index by varying the initial n from 1.0 to 4.0 and found that varying the initial Sérsic index does not affect the final fitting results ($\Delta n/n < 0.05$). Other initial guess parameters for the fit are outputs from the SExtractor. The noise for each pixel required for deriving the errors is determined from the variance maps produced during the drizzling process. The PSF used to be convolved with the Sérsic model was obtained by stacking images of unsaturated stars with stellarity index larger than

0.98 and without nearby objects in the z_{850} image.

Examples of GALFIT results are shown in Figure 4. We excluded objects with incredibly large errors obtained from GALFIT, which comprise about 9% of the single-component sBzK galaxies. The unreasonably large errors of some objects indicate the divergence in the fitting process. The number of the remaining single-component sBzK galaxies is 499.

We carried out the Monte Carlo simulations in order to examine the accuracy and reliability of the parameters derived by GALFIT. About 5000 artificial objects were generated for disks ($n = 1$) and spheroids ($n = 4$), with uniformly distributed random magnitudes ($21 - 26$ mag), random effective radii ($0.''01 - 1.''00$), ellipticities ($0.1 - 1.0$), and position angles ($0 - 180°$). The magnitude range was adopted so as to be the same as that of our sample. The artificial galaxies were then convolved with PSF of the z_{850} image and inserted into the observed z_{850} image. GALFIT was performed to the artificial objects in the manner identical to that used for the sBzK galaxies.

Figure 5 shows the resultant accuracy of the output parameters from Monte Carlo simulations with 1σ of distributions
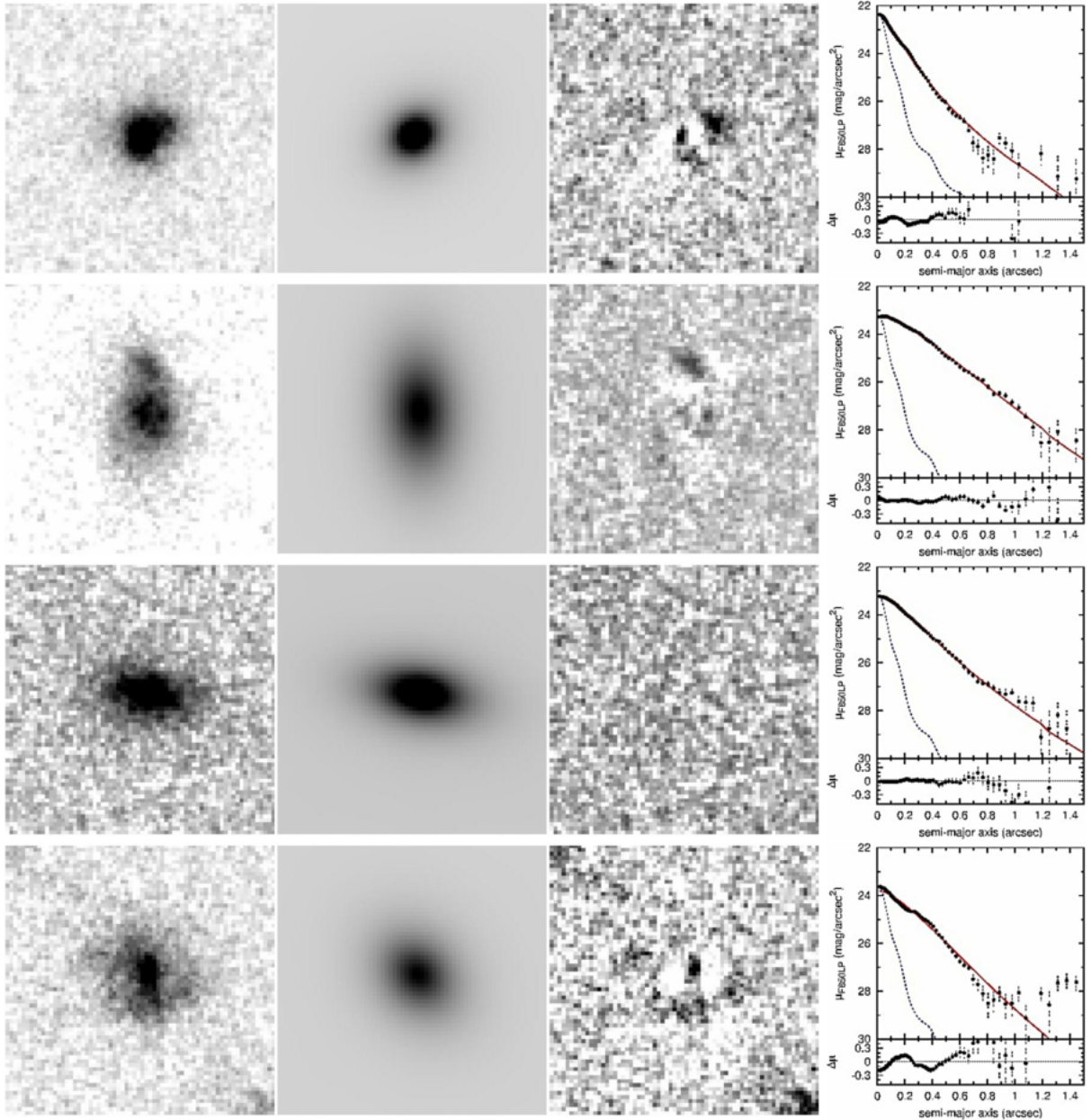
Figure 4. Examples of the 2D surface brightness modeling with GALFIT for the single-component sBzK galaxies. The first (from the left), second, and third panels show the ACS/F850LP image of sBzK galaxies, the best-fitting model constructed by GALFIT, and the residual image, respectively. North is at the top and east is to the left. The size of each image is $2.''0 \times 2.''0$ corresponding to $\sim 17 \times 17$ kpc at $z = 2$. To clearly display the residual part, the residual images are shown with narrower scale range. The rightmost panel shows the azimuthally averaged 1D surface brightness profile of each object (black circles). Red solid and blue dot lines indicate the best-fitting model profile and the PSF, respectively. The bottom of the rightmost panel represents the residual profile of surface brightness.

as a function of the input z_{850} magnitude. The left panel represents the accuracy of the recovered Sérsic indices. Over all range of magnitudes in the simulations ($21 - 26$ mag), the output n distribution has a median value of $\langle n \rangle = 0.96$ with $\sigma_n = 0.68$ for the disks and $\langle n \rangle = 3.49$ with $\sigma_n = 1.34$ for the spheroids. Typical errors on n obtained from GALFIT are 0.02 and 0.06 for the simulated disks and spheroids, respectively. The recovered n is significantly underestimated for the objects with $n = 4$; however, it is possible to distinguish two populations by classifying objects with $n \geq 2.5$ as spheroid-like and those with $n < 2.5$ as disk-like down to $z_{850} = 24.5$ mag. At $z_{850} \sim 25.5$ mag, about half of the input objects with $n = 4$ show output $n \leq 2.5$, but a fraction of the single-component sBzK galaxies fainter than 25.5 mag

is very much small. Nevertheless, keeping this in mind, we also examine the brighter subsample in the subsequent analysis (section 5.3). The right panel of Figure 5, which shows the accuracy of the recovered r_e, indicates that the disk profiles are better recovered than the spheroid profiles. The effective radii of disk profiles are well recovered down to magnitude of 26.0 mag. The typical errors in determining the effective radius are 3% for the disks and 12% for the spheroids in the magnitude range of $20.0 - 26.0$.

4.2. *Results on Sérsic Parameters*

Distributions of effective radius (r_e) and Sérsic index (n) are shown in Figure 6. The effective radius is described in kpc calculated with the photometric redshift. Most of the single-
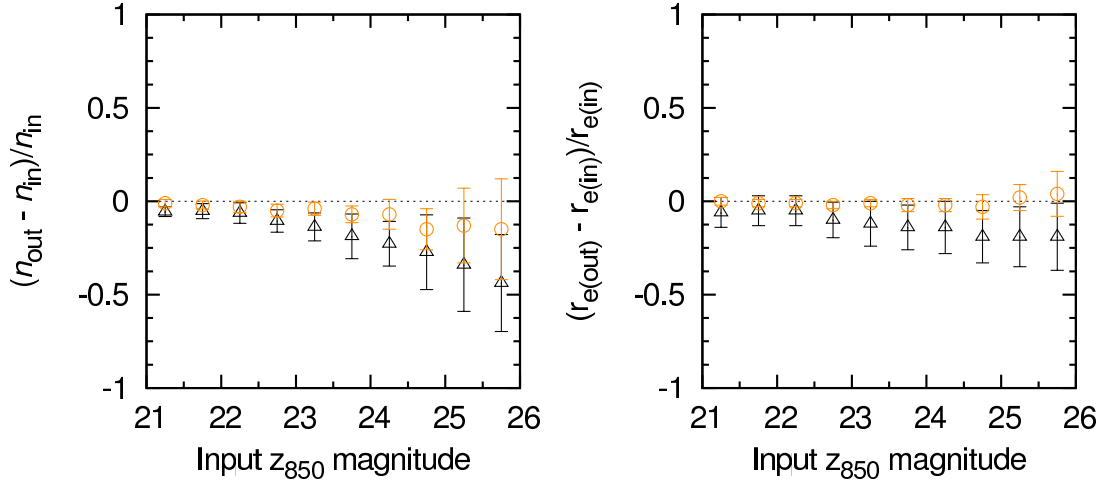
Figure 5. Accuracy of the output parameters from GALFIT based on the Monte Carlo simulations as a function of magnitude for the recovered median Sérsic index (left panel) and median effective radius (right panel). Open circles and triangles refer to artificial objects with an exponential profile ($n = 1$) and those with a spheroid profile ($n = 4$), respectively. Error bars correspond to 1σ of the distribution.

component sBzK galaxies show the effective radius around $1 - 3$ kpc (Figure 6(a)), which is consistent with the previous studies of star-forming galaxies at $z = 2 - 4$ (Overzier et al. 2010; Swinbank et al. 2010). We also show in the figure the distribution for the galaxies with $z_{850} < 24.5$ mag, which is the limiting magnitude at which the structural parameters are well recovered. It is seen that the distributions of both all single-component sBzK galaxies and those with $z_{850} < 24.5$ mag are very similar. In Figure 6(b), the distribution of derived Sérsic index peaks at $n \sim 1$ for both samples. If we refer to a galaxy with $n \geq 2.5$ as a "spheroid-like" object and that with $0.5 \leq n < 2.5$ as a "disk-like" object, we find that 64% (318/499) of the single-component sBzK galaxies are disk-like objects.

In Figure 7, we plot Sérsic index n against effective radius r_e. A slight anti-correlation between the effective radii and the Sérsic indices is seen; galaxies with larger size show smaller Sérsic index. Such a trend can also be seen among Lyman alpha emitters (LAEs) at $z = 3.1$ in the rest-frame UV wavelength (Gronwall et al. 2010). It is interesting to note that the trend is different from the correlation for early-type galaxies in the local universe, where the Sérsic index increases with increasing size (Caon et al. 1993; D'Onofrio 2001; Graham & Guzman 2003; Aguerri et al. 2004; Rothberg & Joseph 2004; Aceves et al. 2006; Kormendy et al. 2009; Ascaso et al. 2011).

Figure 8 shows the effective radius against stellar mass of the single-component sBzK galaxies with $0.5 \leq n < 2.5$ and the relations for local galaxies. Since our analysis is based on the z_{850} image which corresponds to the rest-frame UV wavelength (~ 3000 Å) at $z \sim 2$, it is difficult to compare the results for sBzK galaxies with those for the local galaxies which have been studied in the optical wavelength. In order to make more useful comparison, we corrected the effective radius in the rest-frame UV to that in the rest-frame optical wavelength with $r_{e,opt}/r_{e,UV} = 1.37$, the ratio of median effective radius in the rest-frame UV and optical wavelengths for star-forming galaxies (BM/BX and Lyman break galaxies) at the similar redshift by Swinbank et al. (2010). The stellar masses of the local galaxies are corrected to the Salpeter IMF. It is seen from the figure that the corrected effective radius of the $z \sim 2$ sBzK galaxies slightly depends on their stellar mass; size increases with the stellar mass. Most of the single-

component sBzK galaxies distribute in the region where the local disks or $z \sim 1$ disks studied by Barden et al. (2005) locate (contours). In other words, most of the sBzK galaxies show the surface stellar mass density comparable to the local disks, though some of them show larger surface stellar mass densities that are more typical to the local elliptical galaxies (green line; Shen et al. 2003). These results seem to suggest that most of the single-component sBzK galaxies at $z \sim 2$ already have a disk structure close to that of the present-day disk galaxies.

5. DISTRIBUTION OF APPARENT AXIAL RATIO (B/A) AND INTRINSIC SHAPE OF THE SBZK GALAXIES

5.1. b/a Distribution of the Single-Component sBzK Galaxies

The peak of Sérsic-index distribution at $n \sim 1$ suggests that most of the single-component sBzK galaxies are disk-like. The nature of $n \sim 1$ is usually interpreted as an evidence for a disk galaxy. However, it is important to investigate whether they indeed have a disk shape or not. In the local universe, the intrinsic three-dimensional shape is examined statistically from the distributions of the apparent axial ratios b/a (e.g., Ryden 2004; Vincent & Ryden 2005; Padilla & Strauss 2008; Unterborn & Ryden 2008). In this study, we examine the distribution of the apparent axial ratios of the single-component sBzK galaxies, and compare it with model distribution to constrain their intrinsic shape.

The b/a distribution of the single-component sBzK galaxies with $0.5 \leq n < 2.5$ is shown in Figure 9. The peak of the distribution is at $b/a \sim 0.4$. The b/a distribution of the present-day disks is also shown in Figure 9 just to demonstrate the b/a distribution in case of a round disk shape. The study of a recent, very large ($\sim 303,000$) sample of disk galaxies from the Sloan Digital Sky Survey Data Release 6 (SDSS DR6) by Padilla & Strauss (2008) shows a flat b/a distribution from $b/a \sim 0.2$ to $b/a \sim 0.8$. It is seen that the b/a distribution of the single-component sBzK galaxies is clearly different from that for the local disks; the distribution of the sBzK galaxies is skewed toward low b/a with the peak at $b/a \sim 0.4$. This implies that the single-component sBzK galaxies do not have a round disk structure.
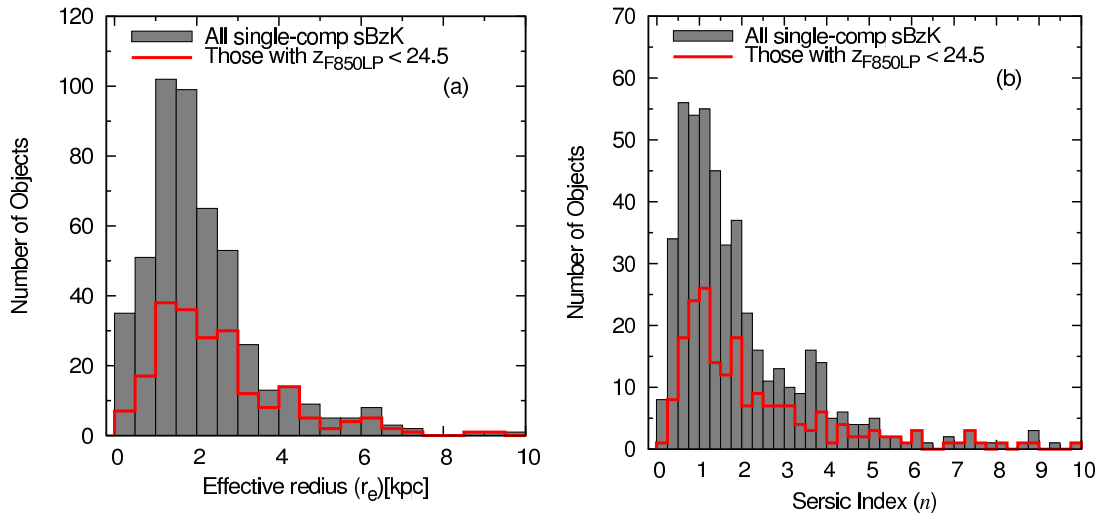
5.2. Bias on b/a Distribution

Figure 6. Distributions of effective radius r_e (left panel) and Sérsic index n (right panel). All 499 single-component sBzK galaxies are shown in the solid black histogram, whereas those with $z_{850} < 24.5$ mag are in the open red histogram.
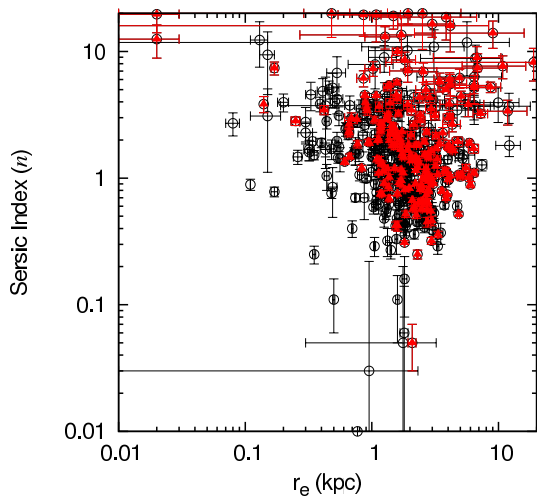

Figure 7. Sérsic index n versus effective radius r_e. Open circles represent all 499 single-component sBzK galaxies and solid triangles show those with $z_{850} < 24.5$ mag.
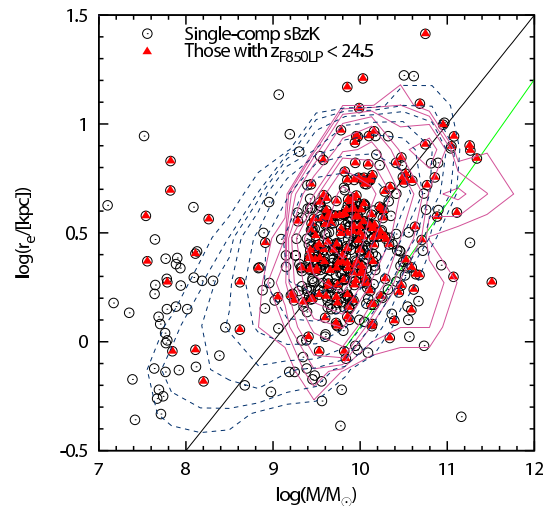

Figure 8. Effective radius and stellar mass of the single-component sBzK galaxies with $0.5 \leq n < 2.5$. The effective radius was corrected according to the ratio of the median effective radius in the rest-frame optical to that in the rest-frame UV wavelengths (see text). The stellar masses of all samples are corrected to the Salpeter IMF. Dashed and solid contours indicate the distributions of $z \sim 0$ and $z \sim 1$ disk galaxies by Barden et al. (2005), respectively. The black solid line represents the average surface density measured from the disk galaxies at $z = 0 - 1$ ($\log \Sigma_M = 8.50$ with $q = 0.5$; Barden et al. 2005). Green line shows the size-mass relation of early-type galaxies from the Sloan Digital Sky Survey (SDSS) by Shen et al. (2003).

Because edge-on galaxies tend to show brighter surface brightness than face-on galaxies at the same magnitude, our sample can possibly be biased toward the edge-on galaxies at faint magnitudes. This may cause the b/a distribution to artificially peak at the lower value. In order to test the selection bias in K band, we generated 10,000 artificial objects with random inclination angles (axial ratios), uniformly distributed magnitudes ($21 - 24$ mag), and random effective radii that are comparable to the actual objects observed in the images at each magnitude bin. After being convolved with the PSF of the K-band image, the artificial objects were inserted into the K-band image and re-detected by using the process identical to that used for real galaxies. Figure 10 shows the resulting detection rate of the artificial galaxies as a function of an input axial ratio. For the artificial objects with $K_{AB} = 21 - 23$ mag, the detection rate is almost constant regardless of the axial ratio and is not lower than 95%. In the faintest magnitude bin ($23 - 24$ mag), the detection rate is $\sim 100\%$ at axial ratio (b/a) of $0.1 - 0.2$ (edge-on) and decreases to $\sim 87\%$ at higher b/a values. Though there is a decreasing trend of the detection rate with increasing b/a, the detection rate remains almost constant from $b/a = 0.3$ to $b/a = 1.0$. Therefore, the

selection bias is unlikely to be the cause for the peak of the b/a distribution of the single-component sBzK galaxies.

We also tested this with the z_{850} image. We generated 5,000 artificial objects with various magnitudes and effective radii for each model of an exponential disk and an exponential disk plus $r^{1/4}$ bulge (disk+bulge). The disk+bulge profile was constructed by assuming the bulge-to-disk ratio (B/D) of 0.5. The ratio of effective radii of bulge against disk is assumed to be 0.1, which is an average ratio for local galaxies in B band (de Jong 1996). The artificial objects were analyzed in the same manner as for the sBzK galaxies, i.e., fitting with a single Sérsic profile. The comparisons between the input and the recovered axial ratios are shown in Figure 11 for disk (left panel) and disk+bulge (right panel) profiles. The axial ratios are well recovered in $z_{850} = 23 - 24$ mag as seen in the both models. The scatter becomes larger at
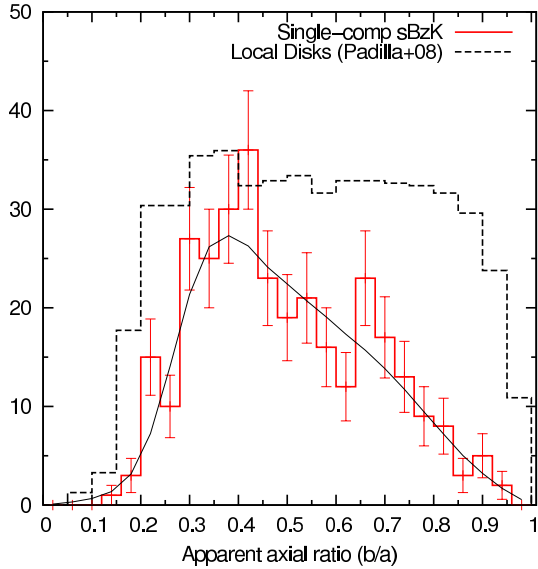
Figure 9. Distributions of the apparent axial ratios (b/a) of the single-component sBzK galaxies and the local disk galaxies (Padilla & Strauss 2008). The observed b/a distribution of sBzK galaxies with $0.5 \leq n < 2.5$ is shown with red solid histogram and the best-fitting model distribution is indicated by black solid line. Dashed line represents the observed b/a distribution of the local disk galaxies (Padilla & Strauss 2008). The distributions are normalized so that they have the same peak.
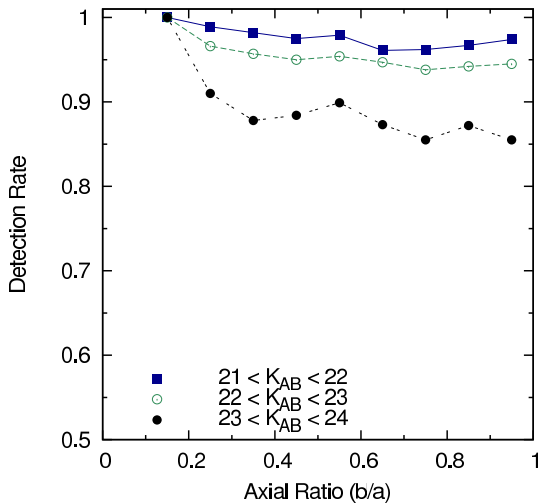

Figure 10. Detection rate of artificial objects in the K-band image as a function of an apparent axial ratio (b/a). Different lines indicate the detection rate of objects in different magnitudes.

the fainter magnitudes, but no artificial effect which increases the number of output b/a around 0.4 is seen in either disk or disk+bulge case. Therefore, the peak of the recovered axial ratio at $b/a \sim 0.4$ seen in our sBzK sample is considered to be real.

5.3. *Intrinsic Shape of the Single-Component sBzK Galaxies*

To examine the intrinsic shape of the sBzK galaxies, we employ the same method as that used for the local disk galaxies. Ryden (2004) modeled a galaxy as a triaxial ellipsoid with major axis A, middle axis B, and minor axis C parameterized by two quantities: disk ellipticity ($\epsilon \equiv 1 - B/A$) and disk thickness (C/A). They then fitted the model with the observed distribution of apparent axis ratios. Following Ryden (2004), we adopted a model in which the disk ellipticity is as-

Table 1
Grids of Model Parameters

Parameter	Minimum value	Maximum value	Steps
μ (B/A)	-4.00 (0.98)	-0.10 (0.01)	0.15
σ	0.20	2.00	0.15
μ_γ	0.10	0.98	0.02
σ_γ	0.01	0.35	0.02

sumed to have a lognormal distribution with mean μ ($\equiv \ln \bar{\epsilon}$) and dispersion σ, while the disk thickness has a Gaussian distribution with mean μ_γ and standard deviation σ_γ. These four parameters μ, σ, μ_γ and σ_γ give a distribution of the intrinsic shapes of galaxies. By randomly selecting an ellipticity and a disk thickness from the distribution, we can compute the apparent axis ratio of b/a (Binney 1985) at a random viewing angle (θ, ϕ) using equations (12)–(15) in Ryden (2004). Repeating this calculation 5000 times, we obtain a model distribution of apparent axial ratio b/a, which is used to compare with the observed distribution of our sample.

We constrained the parameter set of μ, σ, μ_γ, and σ_γ by fitting with the observed distribution of b/a. Ranges and steps of the parameters examined are listed in Table 1. The intrinsic B/A ratio corresponding to the μ parameter is also shown in the parenthesis. The best-fitting set of parameters was obtained by χ^2 minimization. We used a bin size of $\Delta(b/a) = 0.04$ for both the observed and model distributions of b/a. Once we had the best-fitting results, we repeated the fitting analysis with a finer grid centered on the best-fitting values. This refinement was done twice.

For the b/a distribution of 318 single-component sBzK galaxies with $0.5 \leq n < 2.5$, the final best-fitting parameters are $\mu = -0.95^{+0.20}_{-0.15}$, $\sigma = 0.50^{+0.45}_{-0.15}$, $\mu_\gamma = 0.28^{+0.03}_{-0.04}$, and $\sigma_\gamma = 0.060^{+0.020}_{-0.015}$ with $\chi^2_\nu = 0.98$. The errors are at 68% confidence level based on Monte Carlo realization; we re-derived the best-fitting parameters and repeated it 500 times by varying the observed distribution of b/a within their Poisson noises. The model distribution of the best-fitting parameters is also shown with the observed one in Figure 9. The best-fitting $\mu = -0.95$ corresponds to the mean and the peak intrinsic B/A ratio of 0.61 and 0.70, respectively. It is indicated that the intrinsic shape of the single-component sBzK galaxies is more likely to be bar-like or oval, rather than being round.

Figure 12(a) shows the observed distributions of the axial ratios together with the best-fitting model and with 1σ deviated models ($\mu = -0.95^{+0.20}_{-0.15}$). The 1σ deviated models well bracket the observed distribution of apparent axial ratios. Figure 12(a) also shows that the parameter μ varies the b/a distribution in the right part of the peak; the frequency of b/a in the part increases with decreasing μ (i.e., increasing B/A). Changing σ affects the shape of the b/a distribution in both sides of the peak, but the effect is not so large (Figure 12(b)). The μ_γ parameter affects the peak value of the b/a distribution as seen in Figure 12(c). The peak of the apparent axial ratios increases with increasing the disk thickness. The σ_γ parameter slightly affects the b/a distribution around the peak (Figure 12(d)).

We divide the sample of the single-component sBzK galaxies into groups according to their properties and show their b/a distributions in Figure 13. As mentioned above, dividing disk-like and spheroid-like objects at $n = 2.5$ is efficient
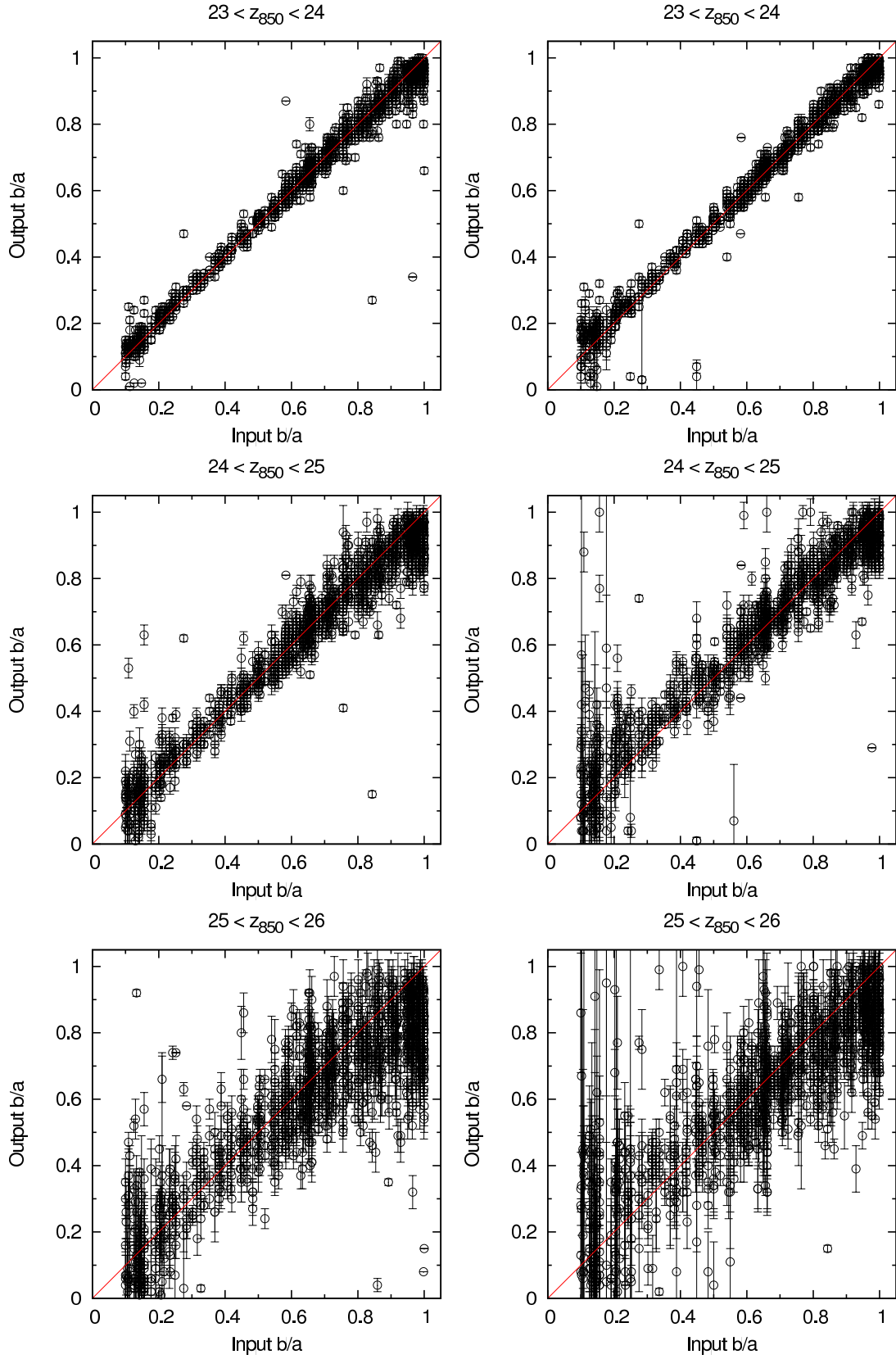
Figure 11. Comparisons between input and recovered axial ratios (b/a) of artificial disk objects (left panel) and disk+bulge objects (right panel) in z_{850} image.
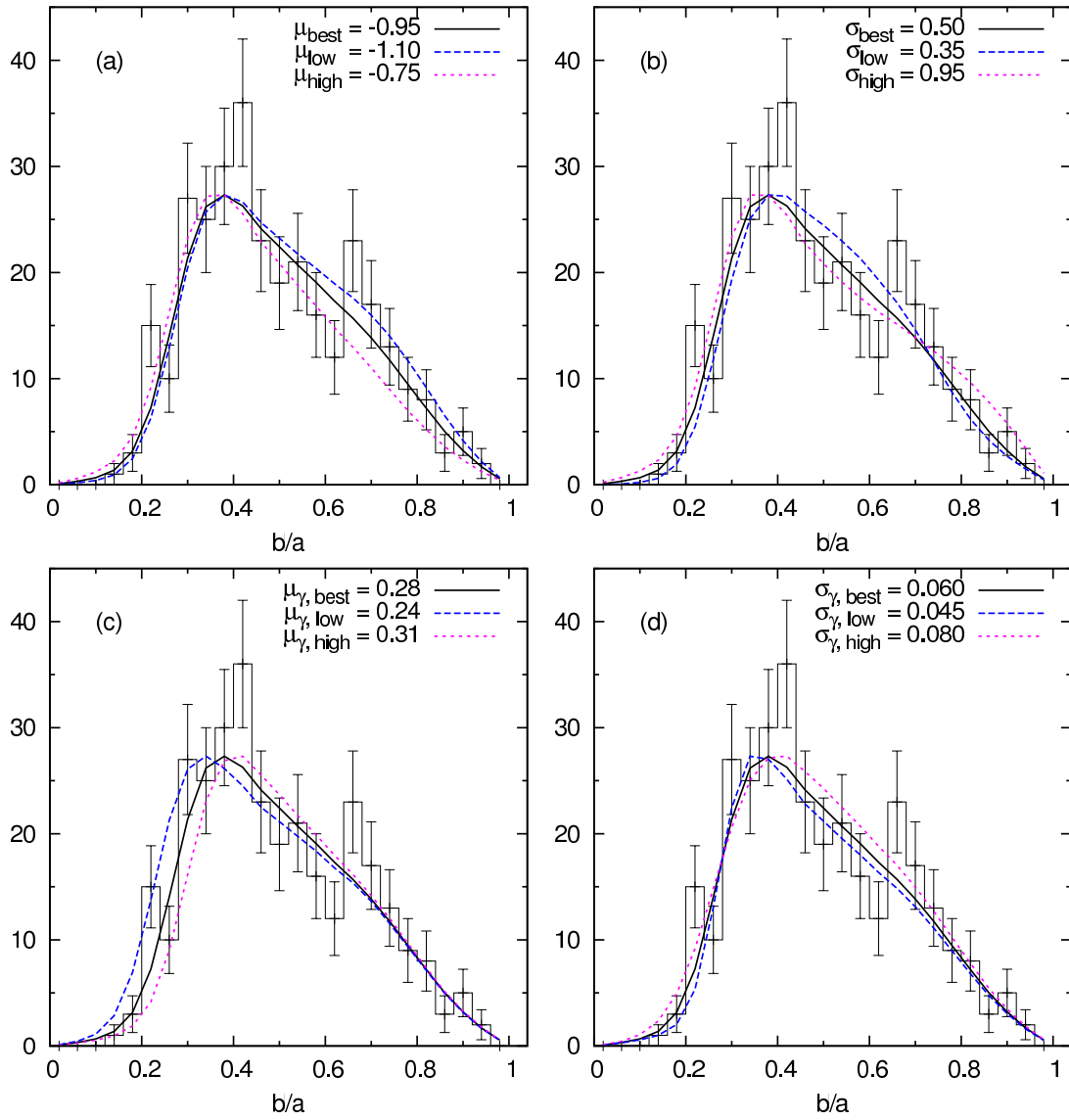
Figure 12. Normalized distributions of the apparent axial ratios by varying model parameters. From Figures (a) to (d), we vary μ, σ, μ_γ, and σ_γ, respectively, with 68% confident interval.
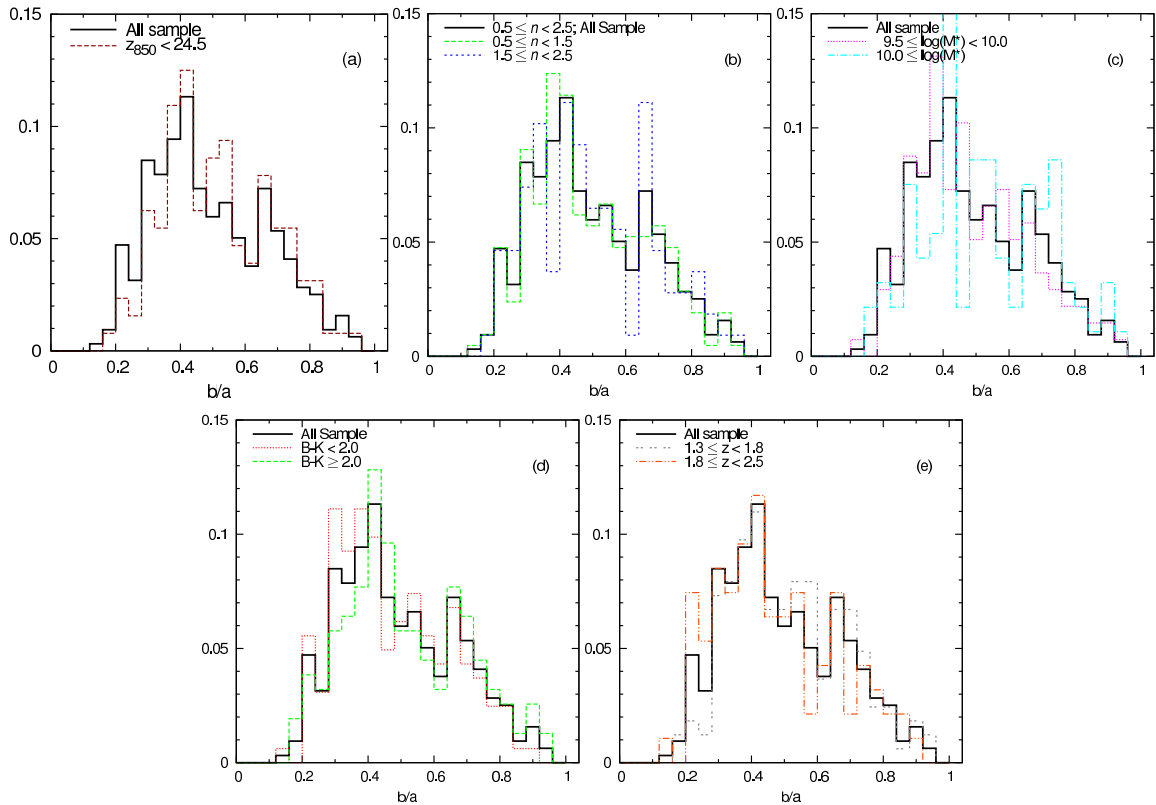
Figure 13. Distributions of the apparent axial ratios of sBzK subsamples. The whole sample of the single-component sBzK galaxies with $0.5 \leq n < 2.5$ is indicated by a solid line in all figures. Figure (a) shows the subsample of sBzK galaxies with $z_{850} < 24.5$ mag. We divide the galaxies with $0.5 \leq n < 2.5$ into subsamples according to their Sérsic index and their stellar mass in figures (b) and (c), respectively. Figure (d) shows the b/a distribution of the subsamples divided by their $B - K$ color. The subsamples are divided so that they have approximately the same number of galaxies. Figure (e) shows distributions of subsamples divided by their photometric redshifts. Ranges of redshifts are selected so that both subsamples are in the comparable comoving volume. The histograms are normalized so that the area is unity.

down to $z_{850} < 24.5$ mag. Because the magnitudes of our sample distribute to $z_{850} \sim 26$ mag, we make a subsample of sBzK galaxies with $z_{850} < 24.5$ mag. Figure 13(a) shows no significant difference of the b/a histogram between the sBzK galaxies with $z_{850} < 24.5$ and $z_{850} < 26.0$ (the whole sample). Their best-fitting parameters are also consistent with each other as summarized in Table 2. Figure 13(b) shows the distributions for subsamples divided by their Sérsic index ($0.5 \leq n < 1.5$ and $1.5 \leq n < 2.5$). The distributions of the subsamples and the whole sample are very similar. Their best-fitting parameters agree with those of the whole sample almost within 1σ (Table 2). Figure 13(c) shows the distributions of the apparent b/a for stellar mass subsamples ($10^{9.5}M_\odot \leq M_{\mathrm{stellar}} < 10^{10}M_\odot$ and $10^{10}M_\odot \leq M_{\mathrm{stellar}}$). The distribution of subsample with $10^{9.5}M_\odot \leq M_{\mathrm{stellar}} < 10^{10}M_\odot$ is similar to that of the whole sample, while there seems to be a slight difference between the whole sample and the objects with $M_{\mathrm{stellar}} \geq 10^{10}M_\odot$. However, the best-fitting parameters listed in Table 2 are in agreement mostly within 1σ errors, though the errors are rather large for some parameters. Figure 13(d) illustrates the distributions of the sBzK galaxies divided by their $B - K$ color ($B - K < 2.0$ and $2.0 \leq B - K$). Both $B - K$ subsamples show the similar distributions to the whole sample. Table 2 also indicates that their intrinsic shape parameters agree with those of the whole sample. Finally, we divide the sample according to the photometric redshift ($1.3 \leq z_{phot} < 1.8$ and $1.8 \leq z_{phot} < 2.5$) in Figure 13(e). No significant difference between the distributions of subsamples and the whole sample is seen from either

Figure 13 or Table 2, suggesting no significant evolution in the redshift range which is about one Gyr separation.

6. POSSIBLE ORIGIN AND EVOLUTION OF THE BAR-LIKE STRUCTURE

Our analysis of the axial ratio distribution shows that the single-component sBzK galaxies have a bar-like or oval structure. At this redshift, the outermost isophote of $\mu_{z850} \sim 28.0$ mag arcsec^{-2} which we reach in this study corresponds to $\mu_B \sim 23.5$ mag arcsec^{-2} at $z \sim 0$ by considering the cosmological dimming and the average $z_{850} - J$ color of the sample objects. This roughly corresponds to the surface brightness just beyond the bar end of present-day galaxies (e.g., Ohta et al. 1990). Are these direct progenitors of present-day barred galaxies? This is unlikely, because the fraction of barred galaxies decreases with increasing redshifts up to $z \sim 1$ (van den Bergh et al. 1996, Abraham et al. 1999, Sheth et al. 2008). Although there has been a debate on the evolution of the bar fraction among disk galaxies, a recent study with a large sample taken with HST/ACS shows that the bar fraction drops to $\sim 10 - 20\%$ at $z \sim 0.84$ (Sheth et al. 2008). Sheth et al. (2008) pointed out in massive galaxies ($\gtrsim 10^{11}M_\odot$) at $z \sim 0.8$ that the fraction is as large as in local massive galaxies, but in our sample such massive galaxies are rare and most of the sample galaxies have stellar mass less than $10^{11}M_\odot$ (Figure 3). It is also worth noting here that the axial ratio distribution of nearby barred galaxies is rather flat (Ohta et al. 1990).

The radial surface brightness distributions of the single-component sBzK galaxies and their intrinsic axial ratios are

Table 2
Best-Fitting Results of Intrinsic Shape for Subsamples of sBzK Galaxies

Subsamples	μ	σ	μ_γ	σ_γ
The whole sample	$-0.95^{+0.20}_{-0.15}$	$0.50^{+0.45}_{-0.15}$	$0.28^{+0.03}_{-0.04}$	$0.060^{+0.020}_{-0.015}$
$z_{850} < 24.5$	$-0.85^{+0.75}_{-0.45}$	$0.50^{+0.90}_{-0.30}$	$0.32^{+0.24}_{-0.06}$	$0.050^{+0.140}_{-0.040}$
$0.5 \leq n < 1.5$	$-0.85^{+0.75}_{-0.30}$	$0.50^{+0.60}_{-0.30}$	$0.30^{+0.06}_{-0.06}$	$0.050^{+0.040}_{-0.040}$
$1.5 \leq n < 2.5$	$-0.85^{+0.75}_{-1.05}$	$0.95^{+0.90}_{-0.75}$	$0.26^{+0.26}_{-0.06}$	$0.050^{+0.240}_{-0.040}$
$9.5 \leq \log(M^*) < 10.0$	$-0.85^{+0.75}_{-0.30}$	$0.50^{+1.05}_{-0.30}$	$0.28^{+0.06}_{-0.04}$	$0.050^{+0.040}_{-0.040}$
$10.0 \leq \log(M^*)$	$-1.30^{+1.20}_{-0.90}$	$0.20^{+1.65}_{-0.00}$	$0.24^{+0.74}_{-0.14}$	$0.070^{+0.280}_{-0.060}$
$B - K < 2.0$	$-0.85^{+0.30}_{-0.15}$	$0.50^{+0.30}_{-0.15}$	$0.28^{+0.02}_{-0.04}$	$0.010^{+0.060}_{-0.000}$
$B - K > 2.0$	$-1.00^{+0.90}_{-0.60}$	$0.80^{+1.05}_{-0.60}$	$0.30^{+0.34}_{0.08}$	$0.070^{+0.240}_{-0.040}$
$1.3 \leq z < 1.8$	$-0.85^{+0.45}_{-0.30}$	$0.50^{+0.45}_{-0.30}$	$0.30^{+0.06}_{0.02}$	$0.010^{+0.080}_{-0.000}$
$1.8 \leq z < 2.5$	$-0.70^{+0.60}_{-0.75}$	$0.80^{+1.05}_{-0.60}$	$0.28^{+0.12}_{-0.08}$	$0.050^{+0.080}_{-0.040}$

similar to those of N-body bars due to the bar instability. The axial ratio (B/A) of the N-body bars is $\sim 0.4 - 0.6$ and ratio (C/A) is $\sim 0.3 - 0.5$ (e.g., Combes & Sanders 1981; Ohta et al. 1990; Athanassoula & Misiriotis 2002). Athanassoula & Misiriotis (2002) examined the morphological differences of bar structures formed in various disk models. The shape of the bar structure in their massive disk model (MD model), where disk dominates in the inner part of a galaxy, shows a good similarity with the statistical intrinsic shape of the sBzK galaxies. Azimuthally averaged radial profiles of the models also show exponential type. Meanwhile, a halo mass dominated model and a massive disk with a central bulge model show much more narrower bar structure with a rather flat-type radial surface brightness distribution, dissimilar to the observed properties obtained in this study. These suggest that the bar-like structure seen in the sBzK galaxies may form by bar instability which takes place when the disk mass fraction against dark halo mass within a disk radius exceeds the threshold (Ostriker & Peebles 1973). If this is the case, a key of the origin of the bar-like structure may be central condensation of baryonic matter as compared with dark matter distribution; massive baryonic disk in a less massive dark matter halo within a certain radius can lead bar instability resulting into such bar-like structure. Although the Q-parameter also plays a role in the bar instability, the shape of the galaxies may be a clue to understand the dynamical formation process of disk galaxies.

Another possible cause for the origin of the bar-like structure may be galaxy interaction and/or merge (e.g., Noguchi 1987). Since many of the sBzK galaxies show multiple structure (46%), this could be a cause. But it should be noted the analyzed sample of the sBzK galaxies are the single-component sBzK galaxies and thus no clear sign for strong close galaxy interaction. A cold gas accretion onto a galaxy halo (e.g., Dekel et al. 2009) may also form an non-axisymmetric structure. However, this kind of cold gas accretion seems to more preferentially occur at an intersection of filamentary structure of the universe, and its effect would be dominated in massive galaxy. Dekel & Birnboim (2006) showed that the cold gas accretion affects in the halo mass larger than $\sim 10^{12} M_\odot$ thus $\sim 10^{11} M_\odot$ in baryonic mass, while the stellar mass of our sample is mostly less than $\sim 10^{11} M_\odot$. Hence this mechanism would not be expected to be dominated in the sBzK galaxies.

The axial ratio distributions peaking at $b/a = 0.4 \sim 0.5$ are seen among Lyman break galaxies at $z \sim 3$ and 4 (Ravindranath et al. 2006) and Lyman α emitters at $z = 3.1$ (Gron-

wall et al. 2010). Although these higher redshift star-forming galaxies, in particular Lyman break galaxies, may not be progenitor of the present-day disk galaxies as mentioned in section 1 and we see their morphology in UV wavelength, these galaxies presumably have similar bar-like structure as the sBzK galaxies, and the origin might be the same as that for the sBzK galaxies.

What is the descendant of the sBzK galaxies? The properties described in section 4 and similarity in size and the stellar mass density point the sBzK galaxies to progenitors of the present-day disk galaxies. However, since they do not show the round-shape disk structure, a transformation from the bar structure to the round disk structure should occur, if the sBzK galaxies really evolved into disk galaxies. The axial ratio distribution of star-forming galaxies at $z \sim 1.2$ is rather flat (Ravindranath et al. 2006), suggesting that galaxies at $z \sim 1.2$ have the round disk structure. If the sBzK galaxies are growing into these galaxies at $z \sim 1.2$, the elapsed time is about $1 - 2$ Gyr from $z = 1.5 \sim 2$ to $z \sim 1.2$. Thus a rapid transformation mechanism is required. One possibility is that they are gas rich and will make a gas rich merge and results into an exponential round-shape disk (e.g., Springel & Hernquist 2005). Alternatively, a bulge or a central mass condensation at the center of galaxy may dissolve the bar structure. A growing central mass condensation with a mass of a few to 10 % of the disk can dissolve the bar structure with a time scale of a few Gyr and the bar structure is totally destroyed after ~ 5 Gyr for the MD-type disk (Athanassoula et al. 2005). Thus the growth of a bulge and/or supermassive black hole at the center of the galaxies may also cause the shape transformation.

7. CONCLUSION

We study the intrinsic structure of star-forming BzK galaxies (sBzK) at $z \sim 2$ in GOODS-North field. 1029 sBzK galaxies were selected down to $K_{AB} < 24.0$ mag. 54% of them shows a single component in the ACS/F850LP image, which covers the rest-frame UV (~ 3000Å) wavelength. Structural parameters of the single-component sBzK galaxies were obtained by fitting the two-dimensional light distributions in the ACS/F850LP image with a single Sérsic profile. We found that most of them show Sérsic index of $n = 0.5 - 2.5$, indicative of a disk-like structure. The effective radii typically range from 1 kpc to 3 kpc. After correcting the effective radii to those in the rest-frame optical wavelength, we found in the stellar mass-size diagram that most of the single-component sBzK galaxies distribute in the same region as $z = 0 - 1$ disk

galaxies by Barden et al. (2005). This indicates that most of the sBzK galaxies show the surface stellar mass density comparable to the local and $z \sim 1$ disks.

The peak of Sérsic-index distribution at $n \sim 1$ and the comparable surface stellar mass density to the local disks suggest that most of the single-component sBzK galaxies are disk-like. We further examined their intrinsic shape by deriving the distribution of apparent axial ratio (b/a) of the sBzK galaxies to see whether they are really disk-like galaxies. The distribution is skewed toward low b/a values with a peak of $b/a \sim 0.4$, in contrast to a flat distribution for round-shape disks. We compared the axial ratio distribution to the model distributions assuming a triaxial ellipsoid model with axes $A > B > C$. The best-fitting parameters correspond to the mean face-on ratio (B/A) of $0.61^{+0.05}_{-0.08}$ and disk thickness (C/A) of $0.28^{+0.03}_{-0.04}$. This indicates that the single-component sBzK galaxies have a bar-like shape rather than a round disk shape.

This bar-like structure is unlikely to be a direct progenitor of present-day barred galaxies, since the fraction of barred galaxies decreases with increasing redshift. The obtained bar structure seems to be similar to that formed through bar instability; if it is the case, the intrinsic shape may give us a clue to understand dynamical evolution of baryonic matter in a dark matter halo. If the sBzK galaxies really evolve to the present-day disk galaxies, some mechanism for shape transformation is required. Gas rich merge or a bulge and/or supermassive black hole growth at the center of the galaxies may be responsible for this shape transformation.

Finally, it is important to note that we studied the intrinsic shape of the single-component sBzK galaxies in the rest-frame UV wavelength, where structure tends to be influenced by star-forming activities. In order to know the distribution of the stellar component, further studies in the rest-frame optical wavelength with high-resolution images taken with HST/WFC3 is desirable.

REFERENCES

Abraham, R. G., Merrifield, M. R., Ellis, R. S., Tanvir, N. R., Brinchmann, J. 1999, MNRAS, 308, 569

Aguerri, J. A. L., Iglesia-Paramo, J., Vílchez, J. M., & Muñoz-Tuñón, C. 2004, AJ, 127, 1344

Akiyama, M., Minowa, Y., Kobayashi, N., Ohta, K., Ando, M., & Iwata, I. 2008, ApJS, 175, 1

Aceves, H., Velázquez, H., & Cruz, F. 2006, MNRAS, 373, 632

Ascaso, B., Aguerri, J. A. L., Varela, J., Cava, A., Bettoni, D., Moles, M., & D'Onofrio, M. 2011, ApJ, 726, 69

Athanassoula, E., Lambert, J. C., & Dehnen, W. 2005, MNRAS, 363, 496

Athanassoula, E., & Misiriotis, A. 2002, MNRAS, 330, 35

Barden, M., et al. 2005, ApJS, 635, 959

Barger, A., J., Cowie, L., L., & Wang, W. -H. 2008, ApJ, 689, 687

Barnes, J. E. 2002, MNRAS, 333, 481

Bertin, E. & Arnouts, S., 1996, A&AS, 117, 393

Binney, J. 1985, MNRAS, 212, 767

Bolzonella, M., Miralles, J. -M., Pelló, R. 2000, A&A, 363, 476

Brinchmann, J., et al. 1998, ApJ, 499, 112

Bruzual, G., & Charlot, S. 2003, MNRAS, 344, 1000

Bundy, K., Ellis, R. S., Conselice, C. J. 2005, ApJ, 625, 621

Calzetti, D., Armus, L., Bohlin, C., Kinney, A.L., Koornneef, J., & Storchi-Bergmann, T. 2000, ApJ, 533, 682

Caon, N., Capaccioli, M., D'Onofrio, M. 1993, MNRAS, 265, 1013

Capak, P., et al. 2004, AJ, 127, 180

Combes, F., & Sanders, R. H. 1981, A&A, 96, 164

Daddi, E., et al. 2004, ApJ, 617, 746

Daddi, E., et al 2005, ApJ, 626, 680

de Jong, R. S. 1996, A&A, 313, 45

Dekel, A., & Birnboim, Y. 2006, MNRAS, 368, 2

Dekel, A., et al. 2009, Nature, 457, 451

D'Onofrio, M. 2001, MNRAS, 326, 1517

Dutton, A. A., et al. 2011, MNRAS, 410, 1660

Fall, S. M., & Efstathiou, G. 1980, MNRAS, 193, 189

Förster Schreiber, N. M., et al. 2006, ApJ, 645, 1062

Förster Schreiber, N. M., et al. 2009, ApJ, 706, 1364

Giavalisco, M., & Dickinson, M. 2001, ApJ, 550, 177

Giavalisco, M., et al. 2004, ApJ, 600, L93

Graham, A. W., & Guzmán, R. 2003, AJ, 125, 2936

Gronwall, C., Bond, N. A., Ciardullo, R., Gawiser, E., Altmann, M., Blanc, G. A., & Feldmeier, J .J. 2010, arXiv.1005.3006v1

Hartley, W. G., et al. 2008, MNRAS, 391, 1301

Hayashi, M., Shimasaku, K., Motohara, K., Yoshida, M., Okamura, S., & Kashikawa, N. 2007, ApJ, 660, 72

Ichikawa, T., et al. 2007, PASJ, 59, 1081

Kajisawa, M., & Yamada, T. 2001, PASJ, 53, 833

Kajisawa, M., et al. 2006, PASJ, 58, 951

Kajisawa, M., et al. 2009, ApJ, 702, 1393

Kong, X., et al. 2006, ApJ, 638, 72

Kormendy, J., Fisher, D. B., Cornell, M. E., Bender, R. 2009, ApJS, 182, 216

Lambas, D. G., Maddox, S. J., & Loveday, J. 1992, MNRAS, 258, 404

Lilly, S., et al. 1998, ApJ, 500, 75

Navarro, J. F., & Benz, W. 1991, ApJ, 380, 320

Navarro, J. F., & Steinmetz, M. 1997, ApJ, 478, 13

Navarro, J. F., & White, S. D. M. 1994, MNRAS, 267, 401

Noguchi, M. 1987, MNRAS, 228, 635

Ohta, K., Hamabe, M., & Wakamatsu, K. 1990, ApJ, 357, 71

Oke, J. B., & Gunn, J. E. 1983, ApJ, 266, 713

Ostriker, J. P., & Peebles, P. J. E. 1973, ApJ, 186, 467

Ouchi, M., et al. 2001, ApJ, 558, L83

Overzier, R. A., Heckman, T. M., Schiminovich, D., Basu-Zych, A., Gonçalves, T., Martin, D. C., & Rich, R. M. 2010, ApJ, 710, 979

Padilla, N. D., & Strauss, M. A. 2008, MNRAS, 388, 1321

Pannella, M., Hopp, U., Saglia, R. P., Bender, R., Drory, N., Salvato, M., Gabasch, A., Feulner, G. 2006, ApJ, 639, L1

Peng, C. Y., Ho, L. C., Impey, C. D., & Rix, H.-W. 2002, AJ, 124, 266

Pickles, A. J. 1998, PASP, 110, 863

Ravindranath, S., et al. 2006, ApJ, 652, 963

Robertson, B, Bullock, J. S., Cox, T. J., Di Matteo, T, Hernquist, L, Springel, V, & Yoshida, Naoki 2006, ApJ, 645, 986

Rothberg, B., & Joseph, R. D., 2004, AJ, 128, 2098

Ryden, B. S. 2004, ApJ, 601, 214

Sales, L. V., Navarro, J. F., Schaye, J., Vecchia, C. D., Springel, V., & Booth, C. M., 2010, MNRAS, 409, 1541

Salpeter, E. E. 1955, ApJ, 121, 161

Sargent, M. T., et al. 2007, ApJS, 172, 434

Scarlata, C., et al. 2007, ApJS, 172, 406

Sérsic, J. L. 1963, BAAA, 6, 41

Sérsic, J. L. 1968, Atlas de Galaxias Australes (Córdoba: Obs. Astron., Univ. Nac. Córdoba)

Shen, S., Mo, H. J., White, S. D. M., Blanton, M. R., Kauffmann, G., Voges, W., Brinkmann, J., & Csabai, I. 2003, MNRAS, 343, 978

Sheth, K., et al. 2008, ApJ, 675, 1141

Springel, V., & Hernquist, L. 2005, ApJ, 622, L9

Steidel, C. C., Giavalisco, M., Pettini, M., Dickinson, M., Adelberger, K. L. 1996, ApJ, 462, L17

Suzuki, R., et al. 2008, PASJ, 60, 1347

Swinbank, A. M., et al. 2010, MNRAS, 405, 234

Unterborn, C. T., & Ryden, B. S. 2008, ApJ, 687, 976

van den Bergh, S., Abraham, R. G., Ellis, R. S., Tanvir, N. R., Santiago, B. X., & Glazebrook, K. G. 1996, AJ, 112, 359

Vincent, R. A., & Ryden, B. S. 2005, ApJ, 623, 137

Williams, R. E., et al. 1996, AJ, 112, 1335

Wirth, G. D., et al. 2004, ApJ, 127, 3121

White, S. D. M., & Rees, M. J. 1978, MNRAS, 183, 341

Yoshikawa, T., et al. 2010, ApJ, 718, 112

Yuma, S., Ohta, K., Yabe, K., Shimasaku, K., Yoshida, M., Ouchi, M., Iwata, I., & Sawicki, M. 2010, ApJ, 720, 1016